Chaperonin GroEL–GroES Functions as both Alternating and Non-Alternating Engines

Chaperonin GroEL−GroES Functions as both Alternating and Non-Alternating Engines

Daisuke Yamamoto[1,2,3] and Toshio Ando[1,2]

[1]Department of Physics, Kanazawa University, Kakuma-machi, Kanazawa 920-1192, Japan
[2]CREST, JST, Sanban-cho, Chiyoda-ku, Tokyo 102-0075, Japan
[3]Present address: Department of Applied Physics, Fukuoka University, Nakakuma, Jyonan-ku, Fukuoka 814-0180, Japan
Correspondence to Toshio Ando: tando@staff.kanazawa-u.ac.jp

Abstract

A double ring-shaped GroEL consisting of 14 ATPase subunits assists protein folding, together with co-chaperonin GroES. The dynamic GroEL−GroES interaction is actively involved in the chaperonin reaction. Therefore, revealing this dynamic interaction is a key to understanding the operation principle of GroEL. Nevertheless, how this interaction proceeds in the reaction cycle has long been controversial. Here, we directly imaged GroEL−GroES interaction in the presence of disulfide-reduced α-lactalbumin as a substrate protein, using high-speed atomic force microscopy. This real-time imaging revealed occurrence of the primary symmetric GroEL:$GroES_2$ and second-primary asymmetric GroEL:$GroES_1$ complexes. Remarkably, the reaction was observed to often branch into main and side pathways. In the main pathway alternate binding and release of GroES occurs at the two rings, indicating tight cooperation between the two rings. In the side pathway, however, this cooperation is disrupted, resulting in interruption of the alternating rhythm. From various properties observed for both pathways, we provide mechanistic insight into the alternate and non-alternate operations of the two-engine system.

Abbreviations used: HS-AFM, high-speed atomic force microscopy; 2D, two-dimensional

Introduction

Chaperonins are a structurally conserved class of molecular chaperones that mediate protein folding to the native functional state in cells [1,2]. The best studied chaperonin, *Escherichia coli*. GroEL, is a cylindrical protein complex formed by two heptameric rings stacked back to back, each consisting of identical ATPase subunits [3]. GroEL functions together with the lid-like co-chaperonin GroES. GroES is a single homo-heptameric ring and binds to the ends of the GroEL cylinder depending on the nucleotide state of GroEL. The mechanism of productive protein folding assisted by GroEL and GroES has been studied extensively [4−6]. Nonnative, unfolded proteins with exposed hydrophobic residues bind to GroEL at its apical domain that presents a hydrophobic surface for this binding [7]. Then, the substrate protein is encapsulated into the hydrophilic cavity of GroEL upon its binding to ATP and GroES, accompanied by a large conformational change of GroEL [8,9]. The encapsulated protein can fold in this environment taking several seconds, the time needed for one ATP turnover cycle to be completed in the GroES-bound ring. Subsequently, GroES dissociates and then the substrate protein is released from GroEL. Because the two rings of GroEL are identical, these processes proceed at each ring of GroEL.

However, how the reaction cycle proceeds in the “two-engine” system has long been controversial. In a widely accepted model, it is postulated that only one ring binds GroES throughout the cycle, so that asymmetric GroEL:$GroES_1$ complexes (referred to as the bullet complexes) are exclusively formed in the steady-state ATPase cycle. The origin of this asymmetry has been considered to be negative cooperativity between the rings regarding ATP binding [10−12]. That is, only one ring can bind ATP, resulting in exclusive formation of the bullet complexes because GroES can only bind to the ATP-bound ring [13], although GroES is thought to be able to bind to the ADP−Pi-bound ring as well. Only after the bound ATP is hydrolyzed in the GroES-bound ring (*cis*-ring), the opposite GroES-free ring (*trans*-ring) can bind ATP. Actual ATP binding to the *trans*-ring induces release of GroES, ADP and the encapsulated substrate protein from the opposite ring [14,15], while the second GroES binds to the *trans*-ring to form a new *cis*-ring. Thus, this model has concluded that the two rings of GroEL alternately bind and release GroES and hence alternately function. In another model, however, both rings of GroEL are supposed to be able to bind ATP simultaneously and hence also GroES to form symmetric GroEL:$GroES_2$ complexes (referred to as the football complexes). Several lines of evidence have been provided for the existence of a large

population of the football complexes in the presence of ATP [16−27]. However, this model has not gained broad consensus. This is mainly because the methods used hardly allow directly detecting dynamic molecular events occurring at each ring.

Here, using high-speed atomic force microscopy (HS-AFM) [28,29] we directly observed dynamic GroES association and dissociation events at each ring of individual GroEL molecules during the steady-state ATPase cycle in the presence of disulfide-reduced α-lactalbumin. HS-AFM is now established and has recently been used with great success to visualize protein molecules in dynamic action [30−32]. The GroEL−GroES interaction was previously observed by HS-AFM during the course of establishment of this microscopy [33,34]. However, in these studies GroEL was immobilized in an end-up orientation on a mica surface, making it infeasible to study the two-engine cycle. In the present study, we used streptavidin two-dimensional (2D) crystals as a substrate, onto which GroEL molecules were immobilized in a side-on orientation through the streptavidin-biotin linkage [35]. This system allowed us to study the dynamic GroEL−GroES interaction occurring during the two-engine cycle at a nearly saturating concentration of GroES. The HS-AFM imaging of the GroEL−GroES interaction in the steady-state ATPase cycle revealed various properties of the interaction, and thus, provided mechanistic insight into the two-engine cycle, as follows. The symmetric football complex is primarily formed, while the two engines operate alternately in a main pathway but non-alternately and non-simultaneously in a side pathway. The alternate operation in the main pathway is made possible by inter-ring communications; ATP hydrolysis into ADP−Pi in one ring triggers GroES dissociation from the opposite ring, while the resulting asymmetric bullet structure retards ADP dissociation from the *trans*-ring. This retardation can contribute to providing an enough time for the substrate protein to be released from the *trans*-ring but in turn could possibly result in frequent, incomplete nucleotide replacement of ADP with ATP at the *trans*-ring. By this incomplete exchange, the inter-ring communication is very likely to be vanished, and therefore, the reaction pathway is side-tracked into the side pathway.

Results

Patterns of dynamic GroEL−GroES interaction

For HS-AFM visualization of dynamic GroEL−GroES interaction at the two rings of GroEL, the D490C GroEL mutant biotinylated at Cys490 was immobilized in a side-on

orientation on the streptavidin 2D crystal surface [35,36] (Fig. 1A). Since this surface is highly resistant to nonspecific protein binding [35], GroES appeared in HS-AFM images only when it was bound to the immobilized GroEL. This property allowed for the use of a high concentration of GroES (1 μM), unlike conventional single-molecule fluorescence microscopy. Figure 1B presents HS-AFM images that were captured at ~4 frames/s (fps) for dynamic GroEL−GroES interaction in the presence of ATP and a substrate protein, disulfide-reduced α-lactalbumin (Movie S1). The successive images clearly displayed multiple rounds of GroES association/dissociation events at each ring of GroEL (Fig. 1B,C).

In the repeated cycles, the symmetric football complexes appeared most frequently (~67%), while the bullet complexes appeared moderately (~33%) (Fig. 2A), consistent with a previous electron microscopy study [37]. Next, we analyzed the order of association and dissociation of GroES at the two rings by choosing the bullet complexes as an initial state (Fig. 2B). These dynamic events observed are largely classified into Type I and Type II; in Type I the *cis/trans* states interchange between the two rings after a round of association and dissociation of GroES, resulting in the polarity change between the initial and second bullet complexes, whereas in Type II no *cis*/*trans* interchange occurs, resulting in no change of the polarity. The probabilities of occurrence of Type I and Type II processes are ~0.69 and ~0.31, respectively. These processes mostly proceeded through formation of the football complexes (Fig. 2Bb,Be). In a less extent, no intermediate state appeared in Type I process (Fig. 2Bc). In addition, processes going through the GroES-free state were only rarely observed (Fig. 2Ba,Bd). As described later, the occurrence of the two types of processes, Type I and Type II, is not an artifact that might arise from missing capturing the second bullet complexes possibly due to insufficient temporal resolution but consistent with a previous single-molecule fluorescent microscopy study [21].

Decay kinetics of football and bullet complexes

The football complexes formed in Type I and Type II processes are apparently the same but different species, as revealed by their distinct decay kinetics. The histogram of lifetime for the football complex in Type I process (hereafter we refer to as Type I football) was well fitted to a single-exponential function with a rate constant of $k^{\text{F-I}} = 0.49\ \text{s}^{-1}$ ($\tilde{\chi}^2 = 0.84$, $p > 0.71$) (Fig. 3A, blue line), so that Type-I football decays in the first-order reaction. By contrast, the histogram of lifetime for the football complex in Type II process (we refer to as Type-II football) showed a maximum at ~2 s and was well fitted to a curve obtained for a sequential

two-step reaction with rate constants of $k^{\text{F-II}}{}_1$ = 1.14 s^{-1} and $k^{\text{F-II}}{}_2$ = 0.59 s^{-1} ($\tilde{\chi}^2$ = 1.46, p = 0.054) (Fig. 3B, blue lines; Note S1). This suggests that in Type II process the dissociation of the second bound GroES is likely to be caused by certain reactions occurring in its bound ring with the rate constants, $k^{\text{F-II}}{}_1$ and $k^{\text{F-II}}{}_2$, as the decay process of Type II football is identical to a process that leads to dissociation of the second bound GroES, unlike in Type I process where the decay of Type I football occurs by dissociation of the early bound GroES.

Supposing that Type II football is apparently formed due to missing capturing the bullet complex that occurs on route to the formation of the second football complex, its lifetime should be approximately $2/k^{\text{F-I}}$ = 4.08 s and its decay kinetics should follow a sequential two-step reaction with the same rate constant identical to $k^{\text{F-I}}$ = 0.49 s^{-1}. Because the decay kinetics exhibited by Type II football is largely inconsistent with these features, Type II football is a real entity.

Next, we analyzed the decay kinetics of the bullet complexes to obtain a clue to an origin of the formation of the two types of football complexes. The lifetime of the bullet complex that was followed by Type I football was well fitted to a single-exponential function with a rate constant of $k^{\text{B-I}}$ = 2.75 s^{-1} ($\tilde{\chi}^2$ = 0.48, p > 0.94) (Fig. 3C, blue line). Also the lifetime of the bullet complex that was followed by Type II football was well fitted to a single-exponential function but its rate constant $k^{\text{B-II}}$ was noticeably smaller than $k^{\text{B-I}}$, i.e., $k^{\text{B-II}}$ = 2.02 s^{-1} ($\tilde{\chi}^2$ = 0.52, p > 0.94) (Fig. 3D). Therefore, there are two types of bullet complexes; one (we refer to as Type I bullet) leads to the formation of Type I football and the other bullet (we refer to as Type II bullet) leads to the formation of Type II football. However, the ratio of the rate constants $k^{\text{B-I}}/k^{\text{B-II}} \approx 1.36$ cannot account for the probabilities of occurrence of Type I and Type II footballs (i.e., ~0.67 and ~0.33, respectively), as described below. The rate constants, $k^{\text{F-I}}$ = 0.49 s^{-1} and $k^{\text{B-I}}$ = 2.75 s^{-1}, provide the probabilities of appearance of Type I football and Type I bullet as 0.85 and 0.15, respectively, which is apparently inconsistent with those mentioned above, even considering the presence of Type II process. This discrepancy is due to the finite time observation of the reaction cycle (Note S2).

Type I football could possibly be classified into two subtypes responsible for the formation of Type I and Type II bullet complexes but it is not the case. This is because the rate of first-order transition from Type I football to Type II bullet was nearly identical to that from Type I football to Type I bullet (Fig. S1). This conclusion was also supported by the fact that both Type I and Type II bullets are formed after Type II football, with respective probabilities similar to those of occurrence of Type I and Type II bullets after Type I football (probabilities:

449/671 ≈ 0.67 for Type I bullet formation and 222/671 ≈ 0.33 for Type II bullet formation). In fact, the numbers of events that Type II process occurred in the *n*-th round in succession were 67 (N_2 = 172), 19 (N_3 = 53) and 4 (N_4 = 15), where N_n (n = 2−4) represents the total number of Type I and Type II bullet complexes formed after Type II football in the *n*-th round. Thus, the probability of going through Type II process is approximately kept constant at ~0.33, irrespective of the number of successive rounds of Type II process. As such, the two types of bullet complexes always occur with respective constant probabilities, after either type of football complex.

Kinetic reaction scheme

From above results as well as analyses described below, the reaction scheme for GroEL−GroES interaction in the steady-state ATPase cycle was constructed (Fig. 4). The reaction cycle proceeds through two distinct main and side pathways, where Type-I and Type-II footballs are formed, respectively. Branching into the two pathways occurs at and is determined by the bullet complexes. The main pathway is consistent with a symmetric chaperonin cycle as proposed previously [24]. By contrast, in the side pathway the product formed by decay of Type-II football is the same as the previous bullet regarding the *cis*/*trans*-ring arrangement. That is, the GroES that has been bound since before and when the reaction reaches the branching point never dissociates while the complex is going through the side pathway. Therefore, its residence time, ~7.5 s (or longer when the complex proceeds in succession to the side pathway), is significantly longer than that in the main pathway, ~4.4 s. On contrary, the resident time of the second bound GroES (~2.6 s) in the side pathway, which is identical to the lifetime of Type-II football, is significantly shorter than the residence time of the early bound GroES (> ~7.5 s) as well as the residence time of bound GroES in the main cycle (~4.4 s).

From the values obtained above for $k^{\text{F-I}}$, $k^{\text{B-I}}$, $k^{\text{F-II}}{}_1$, $k^{\text{F-II}}{}_2$ and $k^{\text{B-II}}$ and from the probability of occurrence of Type II bullet, $r \approx 1/3$, we obtained the average cycle time of GroEL−GroES interaction, $\langle T_c \rangle \approx 6.33$ s, in a way described in Note S3. Supposing that 14 ATP molecules are hydrolysed per GroEL molecule during $\langle T_c \rangle$, the steady-state ATPase activity is estimated to be 2.2 s^{-1} per GroEL molecule. This estimated value is somewhat larger than but similar to the value of 1.5 s^{-1} per GroEL molecule measured biochemically for GroEL−GroES in the presence of an unfoldable substrate protein, α-lactalbumin [38], the same substrate protein as that used in the present study.

Type II football in the side pathway shown in pale colors (Fig. 4) indicates an intermediate state that is apparently the same as but different from Type II football initially formed upon GroES binding. Existence of this intermediate state was deduced from the histogram of lifetime for Type II football as mentioned above (Fig. 3B). Regarding Type I football shown in pale colors (Fig. 4), we discuss in the next section.

Kinetics undergone by bound GroES in the main pathway

Previous single-molecule fluorescence microcopy measurements have shown that dissociation of GroES from a GroEL ring occurs in two steps, through formation of one kinetic intermediate [36,39]. In these studies, however, measurements were performed under the condition that only one GroES was bound to GroEL (i.e, at a low concentration of GroES, 4 nM). Here, we examined the kinetics undergone by a bound GroES in the main circular pathway under the condition that the football complexes were predominantly formed in the presence of 1 μM GroES. Figure 3E shows a histogram for the residence time of GroES. As was the case with the previous studies, the distribution of the resident time showed a maximum but significantly deviated from the curve best fitted to a sequential two-step reaction ($\tilde{\chi}^2$ = 1.51, p = 0.016; Fig. 3E, green lines). For details of the residence time analysis, see Notes S4 and S5. It would be most plausible that before final dissociation the bound GroES simply undergoes the first football complex, the following bullet complex and the second football complex in this order. However, the histogram largely deviates from the corresponding curve (Fig. S2). A deviation was also noticed, although in a less extent, even when the histogram was fitted to a sequential three-step reaction without restriction ($\tilde{\chi}^2$ = 0.92, p = 0.60), as depicted in the cumulated number of GroES dissociation events (Fig. 3E, blue lines). In this fitting (Fig. 3E, right, blue line), a significant advance is evident at the initial phase in the lag period, compared to the experimental data (Fig. 3E, right, black dots). Therefore, we postulate that the bound GroES undergoes three intermediates (besides the initial football complex) before its dissociation. The histogram was well fitted to a curve for a sequential four-step reaction with rate constants of k_1 = 0.92 s^{-1}, k_2 = 0.90 s^{-1}, k_3 = 2.81 s^{-1}, and k_4 = 0.51 s^{-1} ($\tilde{\chi}^2$ = 0.70, p = 0.90) (Fig. 3E, solid red lines). The cycle time of the main pathway calculated from the values of these four rate constants and $k^{B\text{-}I}$ becomes 4.89 s, very close to that calculated from the values of $k^{B\text{-}I}$ and $k^{F\text{-}I}$, i.e., $2 \times (1/k^{F\text{-}I} + 1/k^{B\text{-}I}) \sim 4.80$ s.

However, precisely determining four rate constants from one histogram is difficult. In addition, the histogram does not tell the order of reactions corresponding to these four rate

constants. Therefore, we constructed a sequential four-step reaction model by considering several issues, as well as reassessing the histogram under plausible restrictions, as described below. First, the values of k_3 = 2.81 s^{-1} and k_4 = 0.51 s^{-1} are similar to the values of $k^{B\text{-}I}$ = 2.75 s^{-1} and $k^{F\text{-}I}$ = 0.49 s^{-1}, respectively, indicating that the reaction step corresponding to k_3 occurs at decay of the bullet complex, while the reaction step corresponding to k_4 occurs at decay of either the initial or final football. Moreover, the sum of the values of $1/k_1$ and $1/k_2$, ~2.2 s, approximately coincides with $1/k^{F\text{-}I}$ (~2.04 s). It is well known that substrate protein is encapsulated into the internal cavity of GroEL after the binding of ATP and GroES to the *trans*-ring, which instantly induces movement of the apical domain of the newly formed *cis*-ring. This apical domain movement has been reported to occur in 0.56−1.47 s (rate constant, 0.68−1.8 s^{-1}) after ATP addition, depending on particular substrate protein [40]. Since the values of k_1 and k_2 are in this range, either k_1 or k_2 is very likely to represent the rate of encapsulation. Therefore, two successive reaction steps corresponding to k_1 and k_2 occur during the decay of the initial football complex (see Fig. 4). Therefore, the rate constant k_4 can now be assigned to the rate of final dissociation of the second bound GroES (at the decay of the last football complex). However, the dissociation of another (i.e., early bound) GroES from the initial football occurs in one step, suggesting that this GroES dissociation occurs in parallel to the encapsulation reaction as well as the following unspecified reaction (corresponding to either k_1 or k_2) occurring in the opposite ring. Because of $1/k_1 + 1/k_2 \approx 1/k^{F\text{-}I}$, completion of this unspecified reaction must be synchronized with the dissociation of the early bound GroES. Therefore, the encapsulation reaction as well as the apical domain movement does not seem to affect the counter ring. Collectively, we conclude that after GroES binds to a GroEL ring this GroES undergoes the football complex (depicted in pale colors in Figure 4), the following bullet complex and the last football complex, in this order. Following this scheme, we reassessed the histogram for the residence time of GroES under the restriction of $1/k_1 + 1/k_2 = 1/k^{F\text{-}I}$, $k_3 = k^{B\text{-}I}$ and $k_4 = k^{F\text{-}I}$, resulting in k_1 = 1.14 s^{-1} and k_2 = 0.87 s^{-1} ($\tilde{\chi}^2$ = 0.73, p = 0.88). The fitting curve obtained by this reassessment (Fig. 3E, dashed red lines) was nearly indistinguishable from the initial one (Fig. 3E, solid red lines). Note that k_1 = 1.14 s^{-1} is identical to the value of $k^{F\text{-}II}{}_1$.

Discussion

The acquired HS-AFM images of GroEL−GroES interaction in the presence of α-lactalbumin indisputably displayed that the football complexes are indeed primarily formed

during the repeated reaction cycles. Moreover, the HS-AFM images showed that in the main pathway the two rings of GroEL operate alternately, as previously postulated [21,24,25]. Cooperative interactions between the two rings must govern this rhythmic, alternate operation. In a prevailing view [2,4], a negative cooperative effect between the two rings has been considered to inhibit ATP binding to the *trans*-ring until one ATP turnover is completed in the *cis*-ring, resulting in exclusive formation of the bullet complexes in the reaction cycle. Our results are inconsistent with this view. However, this prevailing view has now been somewhat modified by a recent fluorescence cross-correlation spectroscopy study [38]. This study showed that symmetric complexes are formed by 54% (close to our observation, 67%) and 23% in the presence of unfoldable substrate proteins α-lactalbumin and α-casein, respectively, whereas in the presence of foldable substrate proteins they are formed by less than 10% [38]. In the near future, this dependence on substrate proteins should be further assessed using different methods including HS-AFM, because formation of football complexes with populations much larger than 10% has been reported even in the presence of foldable substrate proteins [17−23,26,27]. In another model, although for the case of absence of substrate protein, ADP dissociation from the *trans*-ring has been considered to limit the reaction cycle, resulting in the accumulation of bullet complexes. In fact, when ATP and ADP coexist in solution, ADP has been shown to be bound to the *trans*-ring [20,41]. Moreover, it has been shown that even after the detachment of GroES from the *cis*-ring ADP resides in the same ring [42,43]. However, in a related model, this negative cooperativity effect on the ADP release from the *trans*-ring has been considered to be weakened by substrate protein bound to the same ring. Therefore, binding of ATP and GroES to the *trans*-ring is accelerated [24,41], and hence, the football complex is considered to be formed during the chaperonin cycle [22,25].

However, as shown in our HS-AFM observation, Type I bullet stays for $1/k^{\mathrm{B\text{-}I}} \sim 0.36$ s even in the presence of substrate protein and 1 μM GroES. This lifetime is much longer than the time required for GroES binding to the ATP-bound *trans*-ring, considering the second-order rate constant for GroES binding in the presence of substrate protein, $1-3 \times 10^7$ $M^{-1}s^{-1}$ [40] and the GroES concentration used here. As such, regarding ADP dissociation, negative cooperativity still effectively acts on the *trans*-ring even in the presence of substrate protein. This suppression of ADP release in the asymmetric bullet complex is reminiscent of handover-hand movement of myosin V on actin; its identical two heads alternately take the leading and trailing positions. This alternate process is made possible by strain-mediated

suppression of ADP release from the leading head [30,44]. Therefore, suppression of ADP release in an asymmetric structure seems to be a common strategy for alternate operation of two-engine ATPase systems.

In the main pathway (see Fig. 4), after binding to the *trans*-ring of GroEL the bound GroES undergoes three intermediates before dissociation (besides the initial football complex itself), as revealed by its residence time analysis. Two of the three intermediates are Type I bullet and the last football complex. This coincidence of the intermediate species indicates that the two rings communicate with each other in these two intermediate states. As to Type I bullet, a negative cooperativity effect exists, as mentioned above. In the final football complex a positive cooperativity effect must also exist that induces the final dissociation of the GroES. In order for this positive cooperative effect to engender, a certain reaction must have proceeded in the opposite ring, until reaching or just before the final dissociation of the bound GroES. During this period, encapsulation of substrate protein into the cavity occurs in the new *cis*-ring but does not seem affect the opposite ring because the encapsulation occurs earlier than the final dissociation of GroES and because this dissociation occurs in one step. The rate of ATP hydrolysis to ADP−Pi in the presence of foldable substrate proteins has been reported to be in the range of 0.31 s^{-1}– 0.36 s^{-1} [39, 45]. Taking into account the higher ATPase activities of GroEL in the presence of unfoldable substrate proteins [38], the value of $k^{F\text{-}I}$ (0.49 s^{-1}) can be considered to correspond to the rate of ATP hydrolysis into ADP−Pi. Therefore, it is very likely that ATP hydrolysis in the new *cis*-ring triggers Pi release and hence final dissociation of GroES from the opposite ring.

To understand the cause of branching into the side pathway, here we summarize its major properties. (i) The early bound GroES never dissociates; rather the newly bound GroES dissociates at the exit of the side pathway, (ii) the formation of Type II bullet leads to the side pathway, (iii) the bullet complex formed at the exit of the side pathway can proceed to either pathway, (iv) the probabilities of branching into the main and side pathways (~2/3 and ~1/3, respectively) cannot be accounted for by the rate constants, $k^{B\text{-}I}$ = 2.75 s^{-1} and $k^{B\text{-}II}$ = 2.02 s^{-1}, (v) the rate of Type II football formation (2.02 s^{-1}) is smaller than that of Type I football formation (2.75 s^{-1}), (vi) Type II football decays in two steps, whereas Type I football decays in one step, (vii) Type II football has a moderately longer lifetime (~2.6 s) than Type I football (~2.04 s), and (viii) importantly the side pathway occurs even in the absence of substrate protein (Fig. 5).

It has been postulated that the substrate protein initially tethered to the apical domain of GroEL would have two or three different fates [46,47]. However, these fates have nothing to do with the pathway branching (Note S6) because the side pathway occurs even in the absence of substrate protein. Although there is no direct evidence at this stage, we consider that incomplete exchange of nucleotide at the *trans*-ring may cause sidetracking into the side pathway, while complete exchange of seven ADPs with seven ATPs assures the GroE system to go through the main pathway. In Type I bullet, the rate of ADP dissociation from the *trans*-ring is suppressed, as described above. This suppression provides an enough time for the substrate protein to be released from the *trans*-ring but in turn could possibly cause frequent, incomplete nucleotide replacement at the *trans*-ring, which would direct the reaction process towards the side pathway. This hypothesis is consistent with partial stochasticity of ATP hydrolysis, as suggested by a previous study [25], as well as with all observed properties of Type II process. For example, the partially remained ADP should somewhat reduce the affinity of the *trans*-ring for GroES, consistent with the smaller rate constant $k^{\text{B-II}} = 2.02\ \text{s}^{-1}$ than $k^{\text{B-I}} = 2.75\ \text{s}^{-1}$. This weaker GroEL−GroES association would possibly reduce the rate of ATP hydrolysis to ADP−Pi in the new *cis*-ring, consistent with the longer lifetime of Type II football than Type I football. Moreover, the hydrolysis of reduced number of ATP molecules in the new *cis*-ring must significantly reduce its positive cooperative effect on the dissociation of the early bound GroES from the opposite ring, consistent with the fact that in the side pathway the early bound GroES never dissociates.

Materials and methods

Proteins

The D490C GroEL was produced by site-directed mutagenesis. D490C GroEL and wild-type GroES were expressed in *Escherichia coli* XL1-Blue and purified as described previously [48]. Purified D490C GroEL was labeled with biotin by the reaction with biotin-$PEAC_5$-maleimide for 30 min at 25ºC as described [35]. The molar ratio of biotin introduced per GroEL subunit was determined to be 0.8 using 4'-hydroxyazobenzene-2-carboxylic acid (Wako Chemicals, Osaka) [49]. Streptavidin and α-lactalbumin were purchased (Wako Chemicals, Osaka and Nacalai Tesque, Kyoto, respectively).

Streptavidin 2D crystals

Streptavidin 2D crystals were prepared on the surface of mica-supported lipid planar bilayer containing biotin-lipid, as described [35]. Briefly, the mica-supported lipid bilayer was first obtained by a vesicle fusion method. After washing the excess lipids, crystallization of streptavidin was performed by deposition of streptavidin (0.2 mg/ml) dissolved in crystallization buffer (10 mM HEPES, 150 mM NaCl and 2 mM $CaCl_2$, pH 7.4) on the lipid bilayer surface, followed by incubation for 2 h. Then, the streptavidin 2D crystals were chemically stabilized by the application of 10 mM glutaraldehyde mixed with the crystallization buffer. After 5 min incubation, the reaction was quenched using 20 mM Tris added to the crystallization buffer.

High-speed atomic force microscopy

Observations were carried out in amplitude modulation mode using a laboratory-built HS-AFM setup [28,29]. Small cantilevers used are custom made by Olympus (spring constant of 0.1 N/m and the first resonant frequency of 0.8 MHz in water). Sharp tips were fabricated on the original tip by electron beam deposition and then by argon-plasma etching. The biotinylated D490C GroEL diluted to 25 nM was applied to the streptavidin 2D crystals. After 3 min incubation, unattached GroEL was washed out with buffer. HS-AFM imaging was performed at an imaging rate of ~4 fps, at 22 ºC in a solution containing 25 mM HEPES-KOH, 100 mM KCl and 5 mM $MgCl_2$, 1 μM GroES, 1 μM bovine α-lactalbumin, 2 mM ATP and 2 mM DTT. For HS-AFM imaging in the absence of substrate protein shown in Fig. 5, bovine α-lactalbumin was omitted from the solution.

Data Analyses

The species of GroEL−GroES complexes were able to be identified by visual inspection of HS-AFM images, thanks to the high resolution images. The analyses of lifetimes of the bullet and football complexes as well as the residence time of bound GroES were performed with a software program constructed using Mathematica 10.2 (Wolfram Research, Illinoi). The histograms of lifetime for Type I football and Type I and Type II bullets were fitted to single-exponential decay functions. The histogram of lifetime for Type II football was fitted to an equation for a sequential two-step reaction (Note S1). The residence time of GroES in the main pathway was fitted to equations of sequential two-step, three-step or four-step reactions (Note S4). The fitting results were also depicted with curves obtained by using corresponding

equations for the cumulated number of events that occur during the period from time Δt to time $n\Delta t$, where n is integer and Δt is the frame time of imaging (Note S4). This depiction provides better inspection for the fitting results than the use of curves for lifetime or residence time distribution. The details of data analysis for sequential three and four-step reactions are described in Note S5.

References

[1] F.U. Hartl, A. Bracher, M. Hayer-Hartl, Molecular chaperones in protein folding and proteostasis, Nature 475 (2011) 324−332.

[2] F.U. Hartl, M. Hayer-Hartl, Molecular chaperones in the cytosol: from nascent chain to folded protein, Science 295 (2002) 1852−1858.

[3] K. Braig, Z. Otwinowski, R. Hegde, D.C. Boisvert, A. Joachimiak, A.L. Horwich, et al., The crystal structure of the bacterial chaperonin GroEL at 2.8 Å, Nature 371 (1994) 578−586.

[4] A.L. Horwich, W.A. Fenton, Chaperonin-mediated protein folding: using a central cavity to kinetically assist polypeptide chain folding, Q. Rev. Biophys. 42 (2009) 83−116.

[5] T.K. Chaudhuri, V.K. Verma, A. Maheshwari, GroEL assisted folding of large polypeptide substrates in *Escherichia coli*: present scenario and assignments for the future, Prog. Biophys. Mol. Biol. 99 (2009) 42−50.

[6] A.I. Jewett, J.E. Shea, Reconciling theories of chaperonin accelerated folding with experimental evidence, Cell. Mol. Life Sci. 67 (2010) 255−276.

[7] D.K. Clare, P.J. Bakkes, H. van Heerikhuizen, S.M. van der Vies, H.R. Saibil, Chaperonin complex with a newly folded protein encapsulated in the folding chamber, Nature 457 (2009) 107−110.

[8] J.S. Weissman, C.M. Hohl, O. Kovalenko, Y. Kashi, S. Chen, K. Braig, et al., Mechanism of GroEL action: productive release of polypeptide from a sequestered position under GroES, Cell 83 (1995) 577−587.

[9] M. Mayhew, A.C. da Silva, J. Martin, H. Erdjument-Bromage, P. Tempst, F.U. Hartl, Protein folding in the central cavity of the GroEL-GroES chaperonin complex, Nature 379 (1996) 420−426.

[10] O. Yifrach, A. Horovitz, Nested cooperativity in the ATPase activity of the oligomeric chaperonin GroEL, Biochemistry 34 (1995) 5303−5308.

[11] S.G. Burston, N.A. Ranson, A.R. Clarke, The origins and consequences of asymmetry in the chaperonin reaction cycle, J Mol Biol 249 (1995) 138−152.

[12] A. Horovitz, K.R. Willison, Allosteric regulation of chaperonins, Curr Opin Struct Biol 15 (2005) 646−651.

[13] Z. Xu, A.L. Horwich, P.B. Sigler, The crystal structure of the asymmetric GroEL-GroES-$(ADP)_7$ chaperonin complex, Nature 388 (1997) 741−750.

[14] H.S. Rye, S.G. Burston, W.A. Fenton, J.M. Beechem, Z. Xu, P.B. Sigler, et al., Distinct actions of *cis* and *trans* ATP within the double ring of the chaperonin GroEL, Nature 388 (1997) 792−798.

[15] H.S. Rye, A.M. Roseman, S. Chen, K. Furtak, W.A. Fenton, H.R. Saibil, et al., GroEL-GroES cycling: ATP and nonnative polypeptide direct alternation of folding-active rings, Cell 97 (1999) 325−338.

[16] M. Schmidt, K. Rutkat, R. Rachel, G. Pfeifer, R. Jaenicke, P. Viitanen, et al., Symmetric complexes of GroE chaperonins as part of the functional cycle, Science 265 (1994) 656−659.

[17] A. Azem, M. Kessel, P. Goloubinoff, Characterization of a functional $GroEL_{14}(GroES_7)_2$ chaperonin hetero-oligomer, Science 265 (1994) 653−656.

[18] H. Sparrer, K. Rutkat, J. Buchner, Catalysis of protein folding by symmetric chaperone complexes, Proc Natl Acad Sci USA 94 (1997) 1096−1100.

[19] A. Koike-Takeshita, M. Yoshida, H. Taguchi, Revisiting the GroEL-GroES reaction cycle via the symmetric intermediate implied by novel aspects of the GroEL(D398A) mutant, J Biol Chem 283 (2008) 23774−23781.

[20] T. Sameshima, T. Ueno, R. Iizuka, N. Ishii, N. Terada, K. Okabe, et al., Football- and bullet-shaped GroEL-GroES complexes coexist during the reaction cycle, J Biol Chem 283 (2008) 23765−23773.

[21] T. Sameshima, R. Iizuka, T. Ueno, J. Wada, M. Aoki, N. Shimamoto, et al.. Single-molecule study on the decay process of the football-shaped GroEL-GroES complex using zero-mode waveguides, J Biol Chem 285 (2010) 23159−23164.

[22] T. Sameshima, R. Iizuka, T. Ueno, T. Funatsu, Denatured proteins facilitate the formation of the football-shaped GroEL-$(GroES)_2$ complex, Biochem J 427 (2010) 247−254.

[23] Takei, Y., Iizuka, R., Ueno, T. & Funatsu, T. Single-molecule observation of protein folding in symmetric GroEL-$(GroES)_2$ complexes. *J. Biol. Chem.* **287**, 41118−41125 (2012).

[24] X. Ye, G.H. Lorimer, Substrate protein switches GroE chaperonins from asymmetric to symmetric cycling by catalyzing nucleotide exchange, Proc Natl Acad Sci USA 110 (2013) E4289−E4297.

[25] D. Yang, X. Ye, G.H. Lorimer, Symmetric GroEL:$GroES_2$ complexes are the protein-folding functional form of the chaperonin nanomachine, Proc Natl Acad Sci USA 110 (2013) E4298−E4305.

[26] X. Fei, X. Ye, N.A. LaRonde, G.H. Lorimer, Formation and structures of GroEL:$GroES_2$ chaperonin footballs, the protein-folding functional form, Proc Natl Acad Sci USA 111 (2014) 12775−12780.

[27] A. Koike-Takeshita, T. Arakawa, H. Taguchi, T. Shimamura, Crystal structure of a symmetric football-shaped GroEL:$GroES_2$-ATP_{14} complex determined at 3.8Å reveals rearrangement between two GroEL rings, J. Mol. Biol. 426 (2014) 3634−3641.

[28] T. Ando, N. Kodera, E. Takai, D. Maruyama, K. Saito, A. Toda, A high-speed atomic force microscope for studying biological macromolecules, Proc Natl Acad Sci USA 98 (2001) 12468−12472.

[29] T. Ando, T. Uchihashi, T. Fukuma, High-speed atomic force microscopy for nano-visualization of dynamic biomolecular processes, Prog Surf Sci 83 (2008) 337−437.

[30] N. Kodera, D. Yamamoto, R. Ishikawa, T. Ando, Video imaging of walking myosin V by high-speed atomic force microscopy, Nature 468 (2010) 72−76.

[31] T. Uchihashi, R. Iino, T. Ando, H. Noji, High-speed atomic force microscopy reveals rotary catalysis of rotorless F_1-ATPase, Science 333 (2011) 755−758.

[32] T. Ando, T. Uchihashi, S. Scheuring, Filming biomolecular processes by high-Speed atomic force microscopy, Chem Rev 114 (2014) 3120−3188.

[33] M.B. Viani, L.I. Pietrasanta, J.B. Thompson, A. Chand, I.C. Gebeshuber, J.H. Kindt, et al., Probing protein-protein interactions in real time, Nat Struct Biol 7 (2000) 644−647.

[34] M. Yokokawa, C. Wada, T. Ando, N. Sakai, A. Yagi, S.H. Yoshimura, et al., Fast-scanning atomic force microscopy reveals the ATP/ADP-dependent conformational changes of GroEL, EMBO J 25 (2006) 4567−4576.

[35] D. Yamamoto, N. Nagura, S. Omote, M. Taniguchi, T. Ando, Streptavidin 2D crystal substrates for visualizing biomolecular processes by atomic force microscopy, Biophys. J. 97 (2009) 2358−2367.

[36] H. Taguchi, T. Ueno, H. Tadakuma, M. Yoshida, T. Funatsu, Single-molecule observation of protein-protein interactions in the chaperonin system, Nat Biotechnol 19 (2001) 861−865.

[37] M. Beiβinger, K. Rutkat, J. Buchner, Catalysis, commitment and encapsulation during GroE-mediated folding, J Mol Biol 289 (1999) 1075−1092.

[38] S. Haldar, A.J. Gupta, X. Yan, G. Miličić, F.U. Hartl, M. Hayer-Hartl, Chaperonin-assisted protein folding: Relative population of asymmetric and symmetric GroEL:GroES complexes, J Mol Biol 427 (2015) 2244–2255.

[39] T. Ueno, H. Taguchi, H. Tadakuma, M. Yoshida, T. Funatsu, GroEL mediates protein folding with a two successive timer mechanism, Mol Cell 14 (2004) 423−434.

[40] F. Motojima, C. Chaudhry, W.A. Fenton, G.W. Farr, A.L. Horwich, Substrate

polypeptide presents a load on the apical domains of the chaperonin GroEL, Proc Natl Acad Sci USA 101 (2004) 15005−15012.
[41] J.P. Grason, J.S. Gresham, G.H. Lorimer, Setting the chaperonin timer: a two-stroke, two-speed, protein machine, Proc Natl Acad Sci USA 105 (2008) 17339−17344.
[42] J.P. Grason, J.S. Gresham, L. Widjaja, S.C.Wehri, G.H. Lorimer, Setting the chaperonin timer: the effects of K^+ and substrate protein on ATP hydrolysis, Proc Natl Acad Sci USA 105 (2008) 17334−17338.
[43] D. Madan, Z. Lin, H.S. Rye, Triggering protein folding within the GroEL-GroES complex, J Biol Chem 283 (2008) 32003−32013.
[44] T.J. Purcell, H.L. Sweeney, J.A. Spudich, A force-dependent state controls the coordination of processive myosin V, Proc Natl Acad Sci USA 102 (2005) 13873−13878.
[45] M. Suzuki, T. Ueno, R. Iizuka, T. Miura, T. Zako, R. Akahori, et al., Effect of the C-terminal truncation on the functional cycle of chaperonin GroEL: Implication that the C-terminal region facilitates the transition from the folding-arrested to the folding-competent state, J Biol Chem 283 (2008) 23931–23939.
[46] F. Motojima, M. Yoshida, Polypeptide in the chaperonin cage partly protrudes out and then folds inside or escapes outside, EMBO J 29 (2010) 4008−4019.
[47] M. J. Todd, G.H. Lorimer, D. Thirumalai, Chaperonin-facilitated protein folding: optimization of rate and yield by an iterative annealing mechanism, Proc Natl Acad Sci USA 93 (1996) 4030−4035.
[48] M. Taniguchi, T. Yoshimi, K. Hongo, T. Mizobata, Y. Kawata, Stopped-flow fluorescence analysis of the conformational changes in the GroEL apical domain, J Biol Chem 279 (2004) 16368−16376.
[49] Y. Kunioka, T. Ando, Innocuous labeling of the subfragment-2 region of skeletal muscle heavy meromyosin with a fluorescent polyacrylamide nanobead and visualization of individual heavy meromyosin molecules, J Biochem 119 (1996) 1024−1032.

Acknowledgements

We thank Prof. Masasuke Yoshida for critical reading of the draft and for valuable comments and Dr. Masaaki Taniguchi for technical assistance. This work was supported by grants to T.A.: KAKENHI, Grant-in-Aids for Basic Research S (#20221006 and #24227005) and Research on Innovative Area (Research in a proposed research area; #26119003) from

Japan Society for the Promotion of Science, and CREST program of Japan Science and Technology Agency.

Appendix A. Supplementary Data

Supplementary data to this article can be found online at http://

Figure legends

Fig. 1. GroEL-GroES interaction observed by HS-AFM. (A) Schematic illustration of the assay system used for HS-AFM imaging of GroEL−GroES interaction. Streptavidin was two-dimensionally crystallized on a mica-supported lipid bilayer surface containing biotin-lipid. D490C GroEL biotinylated at 490C locating at its equatorial domain was immobilized on the streptavidin 2D crystal surface through the biotin-streptavidin linkage. The bulk solution includes 1 μM GroES, 1 μM denatured (disulfide-reduced) lactalbumin and 2 mM ATP. (B) HS-AFM images captured at ~4 fps of GroES binding to and dissociating from the GroEL rings. The dashed lines indicate the positions of toroid ends of the GroEL molecule. The arrowheads indicate GroES bound to GroEL. Z-scale: 15 nm. (C) Time course of the association and dissociation of GroES at each ring of GroEL observed in (B).

Fig. 2. Population of GroEL−GroES complexes and their dynamic appearance and disappearance observed by HS-AFM. (A) Population of species in the presence of 2 mM ATP and 1 μM substrate protein (disulfide-reduced lactalbumin). “n” indicates the total number of frames captured. (B) Patterns and relative proportion of the sequential GroES binding and release events observed during the steady-state ATPase cycle. “n” indicates the total number of events detected.

Fig. 3. Histograms and their best fitting results for lifetime of GroEL−GroES complexes and residence time of bound GroES. The insets in A−E show the cumulated numbers of corresponding events (gray bars) together with curves calculated using rate constants obtained by fitting of their histograms to corresponding models (blue lines for A−D; blue, green and red lines for E). “n” attached to each inset indicates the total number of observed events. (A) Histogram (gray bars) for lifetime of Type I football and the best result of its fitting to a single

exponential function (blue line). (B) Histogram (gray bars) for lifetime of Type II football and the best result of its fitting to a sequential two-step reaction model (blue line). (C) Histogram (gray bars) for lifetime of Type I bullet and the best result of its fitting to a single exponential function (blue line). (D) Histogram (gray bars) for lifetime of Type II bullet and the best result of its fitting to a single exponential function (blue line). (E) Histogram (gray bars) for residence time of GroES and the best result of its fitting to a sequential four-step reaction model (solid and dashed red lines). The dashed red lines show the best result of fitting performed under the restriction of $k_3 = k^{B\text{-}I}$ and $k_4 = k^{F\text{-}1}$, while the solid red lines show the best result of fitting performed without restriction. The green and blues lines show the best results obtained when the histogram for residence time of GroES was fitted to sequential two-step and three-step reaction models, respectively. The inset (right) shows the initial lag-time phase of the cumulated number of GroES dissociation events.

Fig. 4. Kinetic reaction scheme of GroEL−GroES interaction revealed by HS-AFM imaging. The football complexes shown in pale colors are apparently the same as but kinetically different from the respective football complexes initially formed upon GroES binding. The solid black arrows indicate reactions in the main circular pathway, whereas the solid green arrows indicate those in the side pathway. The dashed red arrows indicate reaction processes estimated from the residence time of bound GroES. The order of $k^{F-II}{}_1$ and $k^{F-II}{}_2$ was assigned as shown here, considering the fact that the value of $k^{F-II}{}_2 = 0.59\ s^{-1}$ is smaller than the smallest value reported for the rate of substrate encapsulation reaction that occurs after GroES binding to the same ring of GroEL. The order of k_1 and k_2 was assigned as shown here, considering the fact that the value of k_1 is identical to the value of $k^{F-II}{}_1$. In the side pathway, the coexistence of ATP and ADP in one ring is shown but hypothetical.

Fig. 5. Successive HS-AFM images showing dynamic GroEL−GroES interaction in the absence of substrate protein. The numbers shown are the frame number. As indicated at frame 102, the polarity of the bullet complex is unchanged from the previous bullet (frame 89) after a round of dissociation and association of GroES. Although not shown in this figure, 7 out of total 47 GroES binding and release events observed showed formation of Type II football. The imaging was performed 22 ºC in a solution containing 25 mM HEPES-KOH, 100 mM KCl and 5 mM $MgCl_2$, 1 μM GroES, 2 mM ATP and 2 mM DTT. Imaging rate, ~4 fps; imaging area, 95 × 41 nm^2.

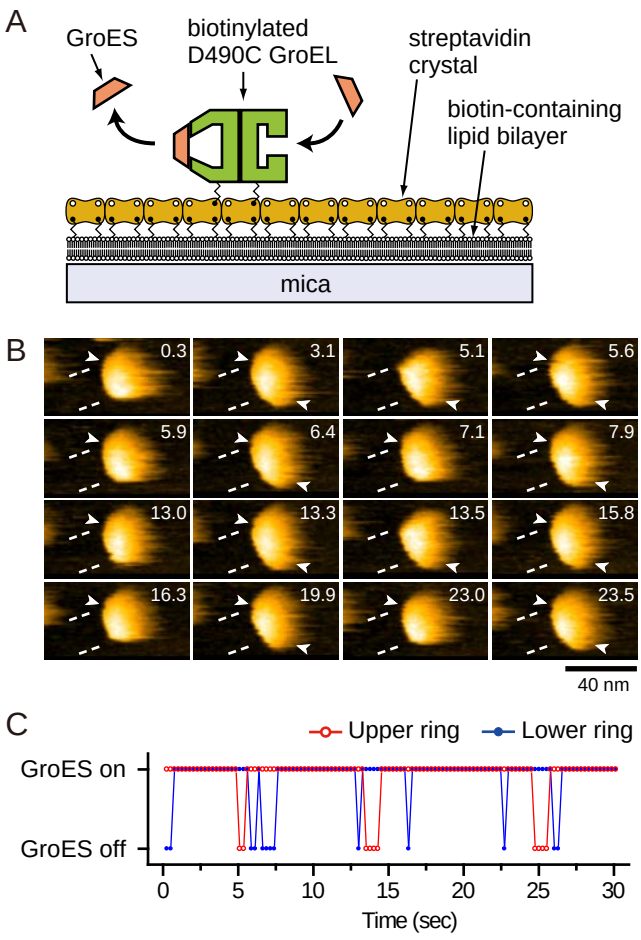
A
GroES
biotinylated
D490C GroEL
streptavidin
crystal
biotin-containing
lipid bilayer
mica
B
0.3
3.1
5.1
5.6
5.9
6.4
7.1
7.9
13.0
13.3
13.5
15.8
16.3
19.9
23.0
23.5
40 nm
C
Upper ring
Lower ring
GroES on
GroES off
0
5
10
15
20
25
30
Time (sec)

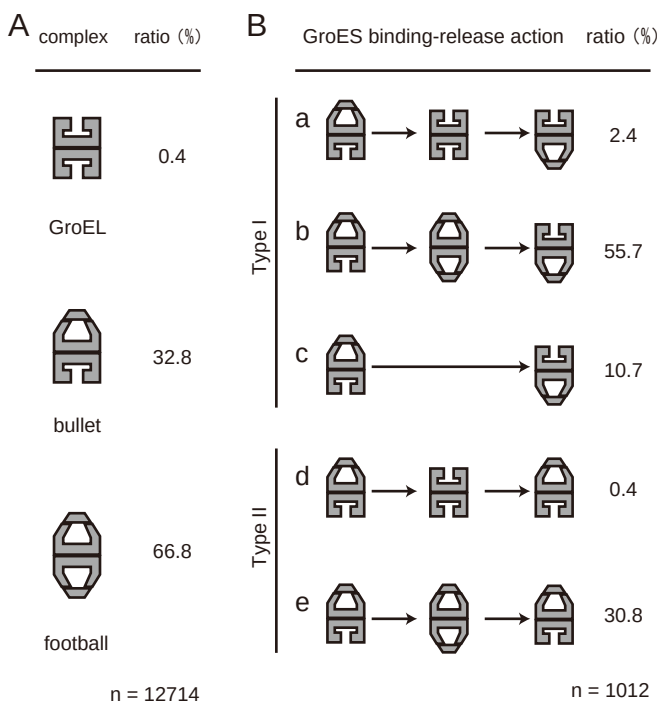
A
complex
ratio（%）
0.4
GroEL
32.8
bullet
66.8
football
n = 12714
B
GroES binding-release action
ratio（%）
Type I
a
2.4
b
55.7
c
10.7
Type II
d
0.4
e
30.8
n = 1012

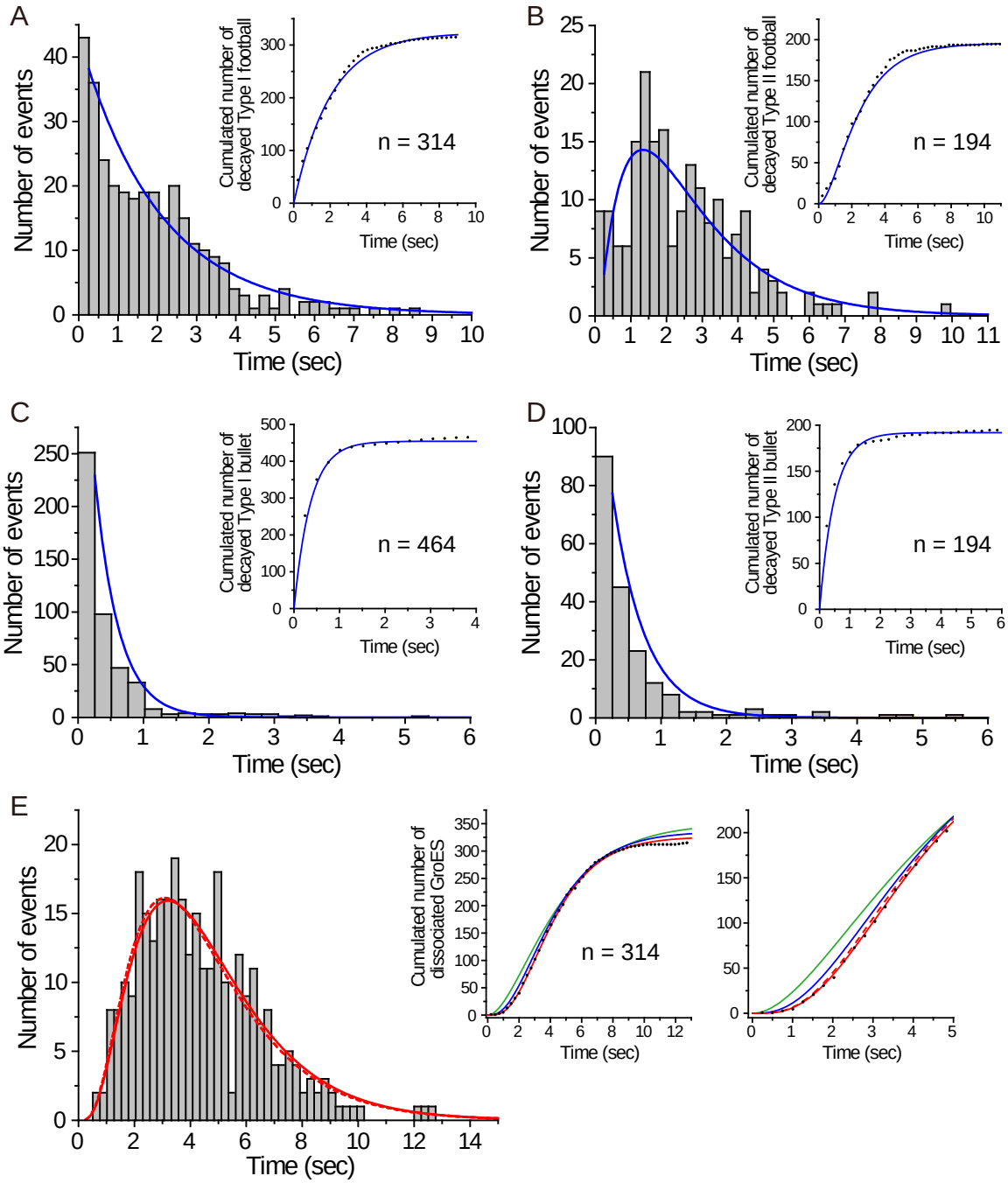
A
Number of events
Time (sec)
Cumulated number of decayed Type I football
n = 314
Time (sec)
B
Number of events
Time (sec)
Cumulated number of decayed Type II football
n = 194
Time (sec)
C
Number of events
Time (sec)
Cumulated number of decayed Type I bullet
n = 464
Time (sec)
D
Number of events
Time (sec)
Cumulated number of decayed Type II bullet
n = 194
Time (sec)
E
Number of events
Time (sec)
Cumulated number of dissociated GroES
n = 314
Time (sec)
Time (sec)

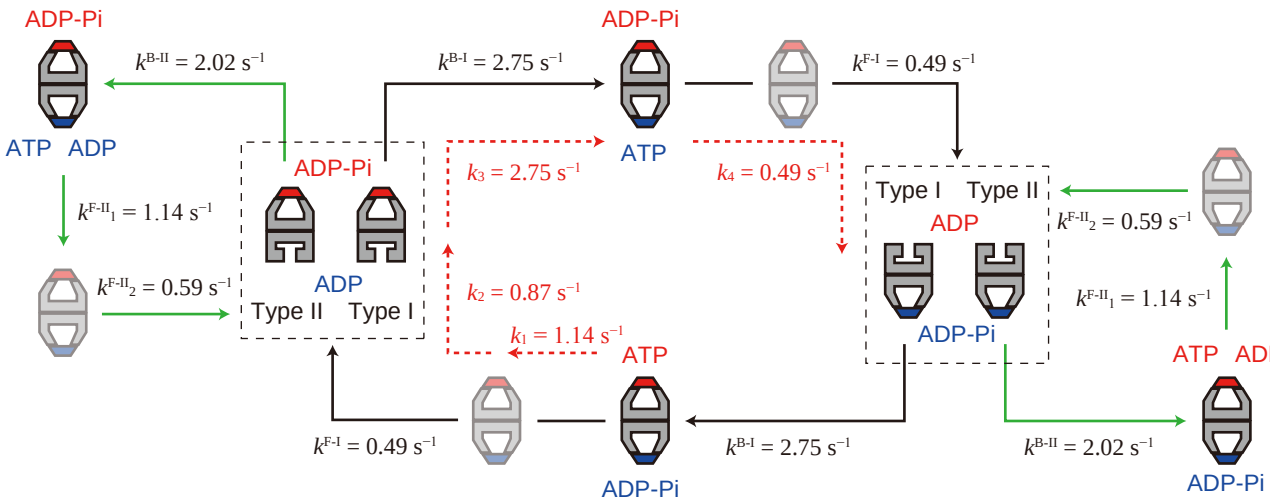
ADP-Pi
$k^{B\text{-}II} = 2.02\ s^{-1}$
$k^{B\text{-}I} = 2.75\ s^{-1}$
ADP-Pi
$k^{F\text{-}I} = 0.49\ s^{-1}$
ATP ADP
ATP
$k^{F\text{-}II}{}_1 = 1.14\ s^{-1}$
ADP-Pi
$k_3 = 2.75\ s^{-1}$
$k_4 = 0.49\ s^{-1}$
Type I Type II
ADP
$k^{F\text{-}II}{}_2 = 0.59\ s^{-1}$
$k^{F\text{-}II}{}_2 = 0.59\ s^{-1}$
ADP
Type II Type I
$k_2 = 0.87\ s^{-1}$
$k^{F\text{-}II}{}_1 = 1.14\ s^{-1}$
$k_1 = 1.14\ s^{-1}$
ADP-Pi
ATP
ATP ADP
$k^{F\text{-}I} = 0.49\ s^{-1}$
$k^{B\text{-}I} = 2.75\ s^{-1}$
$k^{B\text{-}II} = 2.02\ s^{-1}$
ADP-Pi
ADP-Pi

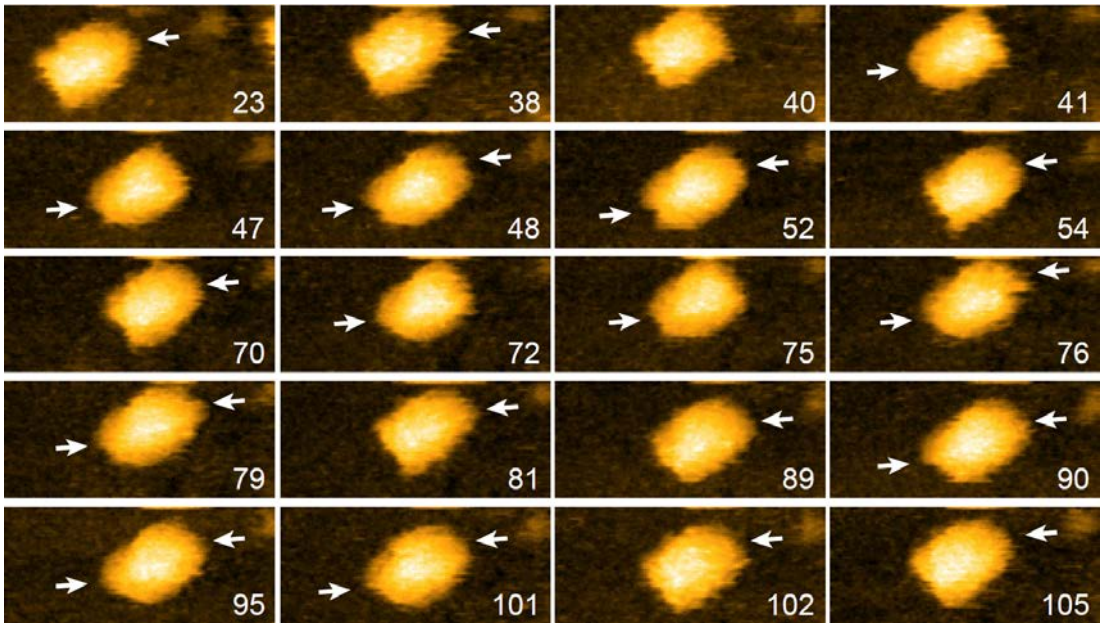
23
38
40
41
47
48
52
54
70
72
75
76
79
81
89
90
95
101
102
105